Spectrum of Engineering Sciences
ISSN (e) 3007-3138 (p) 3007-312X Volume 3, Issue 12, 2025

EFFICIENT REMOVAL OF CADMIUM IONS FROM AQUEOUS SOLUTIONS USING BIMETALLIC SR-CU SUPPORTED GRAPHITIC CARBON NITRIDE COMPOSITE

Nawal Siddique[1], Faryal Ali [2], Aqsa Maqsood[3], Muhammad Ashraf Shaheen[*4], Muhammad Azhar Abbas[5]

[1,*4] *Faculty of Sciences, Superior University Lahore, Lahore 54000, Pakistan*
[2,3] *Institute of Chemistry, University of Sargodha, Sargodha 40100, Pakistan*
[5] *Government Ambala Muslim Graduate College, Sargodha 40100, Pakistan*

[*4]masaheen1964@gmail.com

DOI: https://doi.org/10.5281/zenodo.18031467

Keywords
Sr-Cu@g-C3N4, cadmium removal, bimetallic composite, adsorption isotherm, wastewater treatment

Article History
Received: 11 October 2025
Accepted: 21 November 2025
Published: 23 December 2025

Corresponding Author: *
Muhammad Ashraf Shaheen

Abstract

The contamination of water by cadmium poses serious health and environmental risks, and the use of efficient and cost-effective adsorbents to remove Cd^{+2} in aqueous media is necessary. The synthesis and evaluation of a bimetallic Sr-Cu supported graphitic carbon nitride (Sr-Cu@g-C_3N_4) composite to remove Cd^{+2} in aqueous solutions is discussed here. The composite was made through a simple wet-impregnation process, which ensure evenly distributed Sr and Cu on the g-C_3N_4 surface. To investigate the effects of pH, contact time, initial metal concentration, the dosage of adsorbent and temperature, batch adsorption studies were carried out. The Sr-Cu@g-C_3N_4 was found to have a maximum adsorption capacity of 178 mg g^{-1} in 30 min at pH 6 and 298 K, which was best explained by the pseudo-second-order model, indicating that chemisorption was the most dominant mechanism. The Langmuir isotherm fit the equilibrium data well, which confirmed the monolayer adsorption on a homogeneous surface. Thermodynamic studies indicated that the process is exothermic and spontaneous. The adsorbent also showed five regeneration cycles making it highly effective and thus proving to be practically reusable. In general, Sr-Cu@g-C_3N_4 is a promising, stable, and effective material to use in Cd^{+2} removal during wastewater treatment.

1. Introduction

The removal of toxic heavy metals from contaminated water remains one of the most persistent and high-priority environmental challenges of the 21st century [1]. Rapid industrial expansion, improper waste disposal, and the continuous rise in electronic-waste recycling have all contributed to the increased amount of heavy metals released into water [2]. Among these, cadmium (Cd^{2+}) is recognized as one of the most hazardous pollutants due to its high aqueous mobility, long environmental persistence, and severe bioaccumulation potential. Chronic exposure to $Cd^{2+}$is linked to kidney dysfunction, skeletal degradation, neurological damage, and carcinogenic effects, even at concentrations below regulatory limits [3]. The fact that it is commonly found in effluents of electroplating, pigment

manufacturing, battery manufacturing, and alloy processing highlights the dire necessity of purification technologies that are highly efficient, selective, and cost-effective and can work under realistic environmental conditions [4].

Conventional Cd^{2+} removal methods including precipitation, ion exchange, membrane filtration, and electrochemical treatments, tend to be effective in the laboratory but have severe limitations in application in the real world. These include high operational costs, narrow pH tolerance, membrane fouling, poor selectivity in multi-ion systems, and the generation of secondary waste streams. Adsorption, by contrast, has emerged as a batter alternative due to its operational simplicity, rapid kinetics, potential for regeneration, and adaptability to diverse wastewater matrices [5-14. However, despite extensive research efforts, the development of adsorbent materials that combine high capacity, strong affinity, fast uptake, chemical stability, and recyclability, particularly for Cd^{+2}, remains a formidable challenge [15-19].

In recent years, graphitic carbon nitride ($g\text{-}C_3N_4$) has gained considerable attention as a multifunctional material for environmental applications. The distinctive structure, which consists of tri-s -triazine, gives it a nitrogen (N) based skeleton with the ability to coordinate with metal ions through the electron donor sites. In addition, $g\text{-}C_3N_4$ is chemically robust, thermally stable, inexpensive, and environment friendly. However, pristine $g\text{-}C_3N_4$ suffers from intrinsic limitations that restrict its adsorption performance including low specific surface area, limited porosity, strong interlayer stacking, and less number of high-affinity binding sites. These gaps hinder its ability to take up heavy-metals and motivate the need for strategic material modification. As a result, it has been a primary research goal to improve the quantity and characteristics of active sites on $g\text{-}C_3N_4$ in order to increase metal uptake [20].

To overcome these limitations, recent trends (2024-2025) emphasize metal incorporation, heteroatom doping, surface functionalization, and nanostructure engineering as effective pathways to enhance the adsorption capabilities of $g\text{-}C_3N_4$. Among these strategies, metal loading has emerged as one of the most powerful methods, owing to the ability of metal species to introduce new coordination centers, modulate surface charge distribution, enhance Lewis acidity, and improve electron-transfer interactions. As an example, oxygen-doped $g\text{-}C_3N_4$ g hybridized with molybdenum (Mo) and sulfur (S) enhanced the removal of Cd^{+2} significantly: the modified product had an adsorption capacity of about 294 mg g^{-1}, which is about 8.7 times that of the pure material, and retained more than 94% of its activity in the presence of other ions, including Ca^{+2}, Mg^{+2}, and Zn^{+2} (H. Yin et al., 2024). Mechanistic analysis showed that the new Cd^{+2} species associated with these dopants were formed, showing that selective additives can form stronger and more specific interactions with Cd^{+2}.Transition metals such as copper (Cu) provide strong complexation ability toward heavy metal ions, while alkaline-earth metals such as strontium (Sr) can modify the structural environment, enhance stability, and introduce additional ionic interaction sites. When combined, Sr and Cu can potentially create cooperative binding environments, enabling faster and more selective adsorption processes [21-25].

Despite the progress in modified $g\text{-}C_3N_4$ composites, a clear research gap remains. Most existing studies focus on single-metal modified $g\text{-}C_3N_4$ or investigate heavy-metal removal under narrow experimental conditions. Reports specifically examining bimetallic Sr-Cu functionalization of $g\text{-}C_3N_4$ are extremely limited, and to date, only a small number of studies explore how the synergistic interactions between alkaline-earth and transition metals enhance Cd^{2+} adsorption capacity and selectivity. Furthermore, the mechanistic understanding of how such bimetal-modified sites contribute to surface complexation, electron exchange, and binding-site heterogeneity is still underdeveloped. Additionally, most previous studies neglect essential practical performance indicators including adsorption thermodynamics, kinetic modeling, and applicability across varying pH conditions, tolerance to coexisting ions, and multi-cycle regeneration efficiency. Addressing these gaps is crucial for advancing the real-world applicability of $g\text{-}C_3N_4$ based adsorbents [26-31].

In this context, the present study develops and evaluates a Sr-Cu supported graphitic carbon nitride composite ($Sr\text{-}Cu@g\text{-}C_3N_4$) as a high-performance adsorbent for Cd^{2+} removal from aqueous solutions.

The incorporation of Sr and Cu is hypothesized to introduce abundant active sites, enhance surface electron density, and create synergistic binding centers capable of strongly interacting with Cd^{2+}. Through systematic batch adsorption experiments, the effects of pH, contact time, temperature, initial concentration, and adsorbent dosage are thoroughly investigated. The adsorption behavior is further analyzed using kinetic, isotherm, and thermodynamic models to elucidate the underlying mechanisms governing Cd^{2+} uptake. The study aims not only to demonstrate the superior adsorption performance of Sr-Cu@g-C_3N_4 but also to provide mechanistic insights that can guide the rational design of next-generation bimetallic adsorbents. The findings highlight the potential of Sr-Cu@g-C_3N_4 as a promising candidate for future water purification technologies, addressing both environmental and industrial demands for high-performance heavy-metal remediation materials.

2. Materials and Methods

2.1. Materials

Melamine, copper nitrate trihydrate ($Cu(NO_3)_2.H_2O$, strontium nitrate ($Sr(NO_3)_2$, cadmium nitrate tetrahydrate ($Cd((NO_3)_2.H_2O$ and sodium hydroxide (NaOH) pellets were obtained of analytical grade and used without further purification. All the synthesis and adsorption experiments were performed using deionized (DI) water. All the glassware were pre-soaked with 10 % HNO_3 and washed thoroughly to avoid contamination.

2.2 Synthesis of Graphitic Carbon Nitride (g-C_3N_4)

The synthesis of g-C_3N_4 was thermal polycondensation of melamine [32]. In brief, 100 g of melamine was put in a covered high temperature ceramic crucible and heated to 550 °C in a muffle furnace at a heating rate of 5 °C per min. The resulted pale-yellow cake was ground to form bulk g-C_3N_4.

2.3 Preparation of Sr-Cu@g-C_3N_4 Composite

A simple wet-impregnation strategy was used to prepare the Sr-Cu@g-C_3N_4 composite to ensure that the metal loads on the C_3N_4 surface were uniformly distributed. Firstly, the stoichiometric amount of $Sr(NO_3)_2$ and $Cu(NO_3).23H_2O$ were dissolved in deionized water, creating a clear mixture of metals precursor solution. Individually, a known amount of g-C_3N_4 powder was suspended into this solution and stirred vigorously for 3 h to encourage close interaction between the metal ions and the N-rich environments of the support. pH of the suspension was then gradually changed to about 9 with 0.1M NaOH, which co-precipitated Sr and Cu species onto the g-C_3N_4 surface under controlled conditions. The mixture was aged at 12 h, filtered and washed carefully to eliminate the traces of nitrates followed by drying at 80 °C overnight. Lastly, the dried product was heated at 350 °C under 2 hours to change the deposited metal hydroxides to stable oxide phases and improve their anchorage on the g-C_3N_4 framework. The product, namely Sr-Cu@g-C_3N_4 had been ground into fine powder and stored to be used in adsorption investigations in future.

2.4. Batch Sorption Experiments

The batch adsorption tests were conducted in the ambient laboratory environment to determine the most preferred experimental parameters of the maximum removal of Cd^{2+} by Sr-Cu@g-C_3N_4 composite. A 1000 mg L^{-1} stock solution was prepared by dissolving the necessary amount of $Cd(NO_3)_2$. H_2O in deionized water. The solution was mixed to obtain homogeneity and then the solution was further diluted to obtain the working solution of desired concentrations. pH of each solution was adjusted by adding a 0.1M HCl or 0.5M NaOH, and monitored with a calibrated pH meter. The accurately weighed amount of Sr-Cu@g-C_3N_4 (30mg/ 100ml) was added to 100 mL of Cd^{2+} solution in 250mL of Erlenmeyer flasks, which was agitated at 200 rpm in a thermostatic orbital shaker to ensure homogenous contact between the sorbent and the metal ions.

The effect of various operational parameter on the uptake of Cd^{+2} was systematically investigated. These were solution pH (2-10), contact time (5-60min), initial Cd^{+2} concentration (10-150mg L^{-1}), sorbent dosage (10-60mg) and temperature (298-318K). Equilibrium data was explored using four adsorption isotherms; Langmuir, which represents monolayer adsorption on a homogenous surface; Freundlich, which describe adsorption on a heterogeneous surface; Dubinin -Radushkevich (D-R), which give

information about adsorption energy and mechanism and Elovich, which applies on systems whose adsorption sites are heterogeneous. These models allowed the overall evaluation of adsorption capacity, single surface heterogeneity and binding interactions.

The time-dependent experiments were conducted to determine the equilibrium conditions and how adsorption takes place. To interpret the adsorption mechanism, experimental data were fitted to a set of kinetic models including pseudo-first-order, pseudo-second-order, intraparticle diffusion (Weber-Morris), and pore diffusion (Bangham) to explain the mechanism behind it. All of these models provide information on rate limiting processes, contributions of chemisorption, and diffusional effects. The Gibbs free energy (ΔG°), enthalpy (ΔH°), and entropy (ΔS°) were then determined to evaluate the spontaneity, heat changes, and disorder of the adsorption process. After adsorption Sr-Cu@g-C_3N_4 adsorbent was filtrated and samples' residual dye concentration (Ce) was determined by UV-Vis spectrophotometer at the maximum absorption wavelength for Cd^{+2} (λmax ≈ 228.8 nm). The equilibrium adsorption capacity and removal efficiency (%R) were determined based on Eq. (1) and (2):

$$q_e = \frac{(C_i - C_f)V}{m} \quad (1)$$

$$\%\,\mathrm{Re}moval = \frac{C_i - C_f}{C_i} \times 100 \quad (2)$$

Where: q_e (mg g^{-1}), is the equilibrium sorption capacity, C_e (mg L^{-1}), is the equilibrium concentration represents the initial dye concentration (mg L^{-1}), V (L), is the solution volume and m (g), is the adsorbent mass.

2.5. Regeneration Study

The reusability of o, were tested in terms of successive adsorption-desorption cycles. Following the adsorption experiment of every batch, the Cd^{+2} loaded adsorbent was recovered through filtration followed by washing with deionized water and desorbing with 0.1 M HCl under gentle stirring over 60 minutes. The regenerated adsorbent were washed, dried at 80 °C and reused at the same adsorption conditions. To determine the stability of adsorption behavior and structural integrity of the composite, five cyclic operations were performed in series.

3. Results and Discussion

3.1. Synthesis of Graphitic Carbon Nitride (g-C_3N_4)

The synthesis of g-C_3N_4 was thermal polycondensation of melamine. In brief, 100 g of melamine was put in a covered high temperature ceramic crucible and heated to 550 °C in a muffle furnace at a heating rate of 5 °C per min. The resulted pale-yellow cake was ground to form bulk g-C_3N_4.

3.2. Preparation of Sr-Cu@g-C_3N_4 Composite

A simple wet-impregnation strategy was used to prepare the Sr-Cu@g-C_3N_4 composite to ensure that the metal loads on the C_3N_4 surface were uniformly distributed. Firstly, the stoichiometric amount of $Sr(NO_3)_2$ and $Cu(NO_3).23H_2O$ were dissolved in deionized water, creating a clear mixture of metals precursor solution. Individually, a known amount of g-C_3N_4 powder was suspended into this solution and stirred vigorously for 3h to encourage close interaction between the metal ions and the N-rich environments of the support. pH of the suspension was then gradually changed to about 9 with 0.1M NaOH, which co-precipitated Sr and Cu species onto the g-C_3N_4 surface under controlled conditions. The mixture was aged at 12 h, filtered and washed carefully to eliminate the traces of nitrates followed by drying at 80 °C overnight. Lastly, the dried product was heated at 350 °C under 2 hours to change the deposited metal hydroxides to stable oxide phases and improve their anchorage on the g-C_3N_4 framework. The product, namely Sr-Cu@g-C_3N_4 had been ground into fine powder and stored to be used in adsorption investigations in future

3.3. Batch Sorption Studies

3.3.1. Effect of pH

The effect of solution pH on Cd^{+2} adsorption was investigated within 2-10 pH as shown in Fig.1 (a). At pH 2, adsorption efficiency was relatively low and this can be explained by the fact that excess H^+ ions and Cd^{+2} ions compete strongly over the available adsorption sites as well as the protonation of surface functional groups which suppresses the metal sorbent interactions. Raising the pH to 4 resulted in

a significant effect on the efficiency of the adsorption process, which means that the surface sites began to be deprotonated partially and the electrostatic repulsion decreased.

The highest level of Cd^{+2} adsorption occurred at pH 6 with a with sorption capacity of 178 mg g^{-1} , indicating that near-neutral conditions provide the most suitable surface charge properties to facilitate Cd^{+2} binding. The sorbent surface is mainly negatively charged at this pH which allows the surface and Cd^{+2} to strongly interact electrostatically and form complexes. Minimal reduction in the adsorption efficiency was found at pH 8 and pH 10, which is probably because of the development of cadmium hydroxide species and partial precipitation, which reduce the number of free Cd^{+2} in solution. Based on this, pH 6 was chosen as the best pH to be used in all further adsorption experiments.

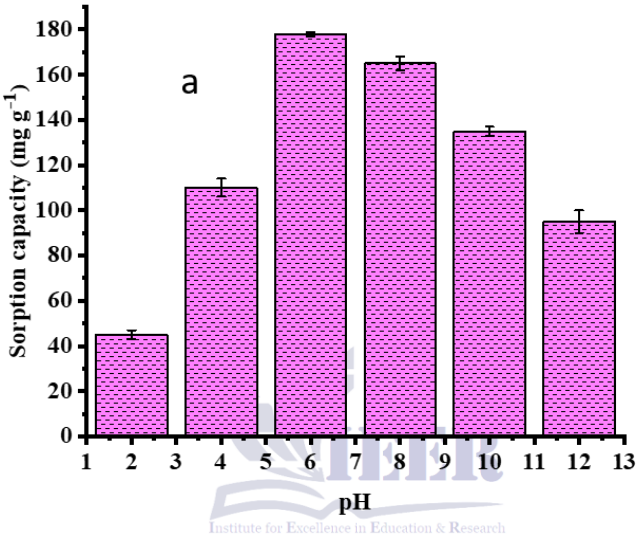

Figure. 1. Effect of pH on Cd^{+2} adsorption onto Sr-Cu@g-C_3N_4composite.

3.3.2. Effect of Sorbent Dosage

The effects of Sr-Cu@g-C_3N_4 dosage on the removal of Cd^{+2} were examined by changing the amount of adsorbent (10-50 mg) in Cd^{+2} solution at pH 6, temperature 298 K, and 30 min contact time. The adsorption capacity was found to rise significantly with increasing dosage between 10 and 30mg as shown in Fig.2a because more active sites of the adsorbent surface were available. At concentrations above

30 mg, the equilibrium adsorption capacity per mg showed a slight decrease, which could be attributed to particle agglomeration, unsaturation at surface sites, and possible competition among active sites, thus decreasing additional Cd^{+2} uptake [33]. As a result, 30 mg was found as the most effective dosage of sorbent, offering high removal efficiency with less amount of sorbent used, making it practical and applicable in real-life and industry-level.

3.3.3. Effect of Initial Metal Ion Concentration

The influence of initial Cd^{+2} concentration on the sorption capacity of Sr-Cu@g-C_3N_4 was investigated by changing the Cd^{+2} concentration in the range of 10 to 150mg L^{-1} under optimum conditions of pH 6, 30mg dose of adsorbent, 298K and contact time 120min. Fig. 2b illustrates that the adsorption capacity increase significantly with the increase of Cd^{+2} concentration, 28.5 to 178mg g^{-1}, reaching maximum at 100mg L^{-1}. This is explained by the fact that the mass-transfer driving force increases with increasing concentration, and thus, at an increased concentration, the diffusion of the Cd^{+2} in the bulk solution to the sorbent surface is accelerated and hence, adsorption increases.

The adsorption capacity reached a plateau beyond 100 mg L^{-1}, which indicates that most of the active sites on Sr-Cu@g-C_3N_4 were occupied by Cd^{+2} ions.

At this point, further uptakes were not achieved as concentration increased further because the binding sites were saturated. This site-limited performance indicates that the initial metal ion concentration has to be optimized to achieve the maximum removal performance as well as to provide efficient use of the sorbent under the practical application.

3.3.4 Effect of Contact Time

The influence of contact time on adsorption of Cd^{+2} onto Sr-Cu@g-C_3N_4 was measured to find out the time required to reach equilibrium. As shown in Fig. 2c, the rate of adsorption was rapid within the first 10-15 minutes, which could be explained by the presence of vacant active sites and the large concentration gradient between the solution and the surface of the sorbent [34]. The equilibrium was reached in 30 minutes with the maximum adsorption capacity of 178mg g^{-1}.

The high rate of initial absorption is attributed to the high amount of unoccupied sites on the adsorbent surface, which easily reacts with Cd^{+2}. As adsorption continued, the total number of vacant sites was reduced and repulsive forces between adsorbed Cd^{+2} and the surrounding solution decreased further, leading to a plateau at equilibrium [35]. It means that Sr-Cu@g-C_3N_4 has a high adsorption rate and could effectively eliminate Cd^{+2} in a short contact time, which is favorable to the practical water treatment process.

3.3.5 Effect of Temperature

Temperature effects on Cd^{+2} adsorption onto Sr-Cu@g-C_3N_4 were examined to explain the thermodynamic properties of the sorption process. The equilibrium adsorption capacity was found to slightly decline with temperature between 298 and 318 298 K, and the maximum adsorption (178 mg g^{-1}) observed at 298 K, as shown in Fig. 2d.

Cd^{+2} ions bind more with the active binding sites on the sorbent surface at low temperatures leading to increased adsorption [36]. As temperature rises, the mobility of Cd^{+2} ions and their faster transport increases with the temperature; this reduces the interactions between the sorbate and the sorbent, decreasing the adsorption efficiency. This tendency shows that the process of Cd^{+2} sorption on Sr-Cu@g-C_3N_4 is exothermic to some extent and suggest that the lower temperatures favors stronger binding of Cd^{+2} ion.

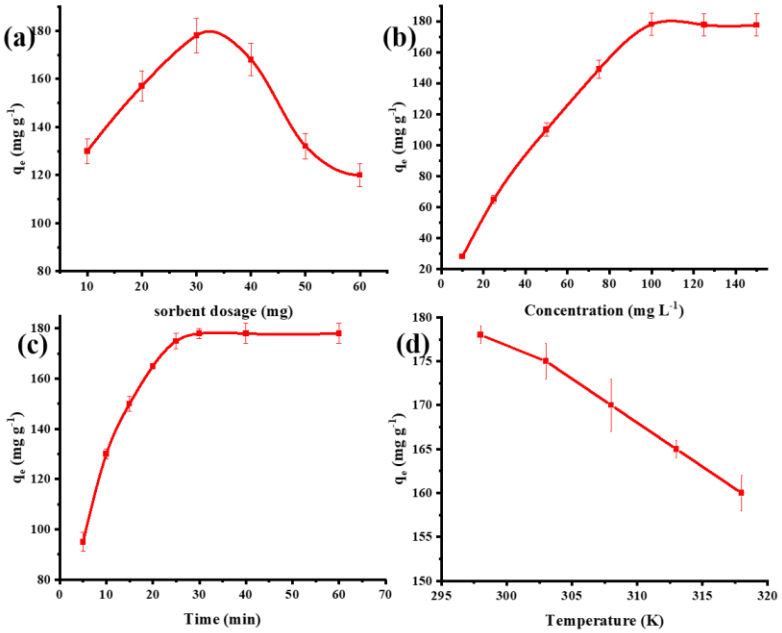

Figure 2. (a) Effect of Sorbent dosage (b) Effect of dye concentration (c) Effect of contact time and (d) Effect of Temperature on Cd^{+2} adsorption onto Sr-Cu@g-C_3N_4composite.

3.4. Isothermal Modeling

Adsorption isotherms are essential in defining the equilibrium distribution of adsorbate molecules at the solid-liquid interface and also the mechanism of adsorption itself [37]. The equilibrium sorption data of Cd^{+2} on the Sr-Cu@g-C_3N_4 composite was examined with four commonly used isotherm models the Langmuir, Freundlich, Dubinin-Radushkevich (D-R) and Elovich models in the current study. The models provide information regarding the surface homogeneity, adsorption capacity, sorption energy and sorbate sorbent interactions. The experimental data obtained under optimized conditions were used to plot the linearized forms of each model, and the plots were created.

3.3.2. Freundlich model

The Freundlich isotherm model describes adsorption on non-uniformly distributed surfaces of heterogeneous surfaces. Its linearized form is given in eq 3.

$$\log q_e = \log K_F + \frac{1}{n}\log C_e \qquad (3)$$

in which, K_F (mg g^{-1}) is the Freundlich constant, which is an adsorption capacity, n is the heterogeneity factor, which is an adsorption strength. The plot of the $\ln q_e$ versus $\ln C_e$ was well-linearized and the correlation coefficient (R^2) was 0.9603, as shown in Fig. 3a. The n was greater than one, which indicated desirable adsorption of Cd^{+2} onto the surface of Sr-Cu@g-C_3N_4 composite (Table 1). However, the comparatively lower value of the R^2 in comparison with the Langmuir model suggests that the multilayer adsorption on the heterogeneous sites makes a relatively small contribution to the general adsorption process.

3.3.1. Langmuir Model

The Langmuir model of isotherm assumes monolayer adsorption on a homogeneous surface with a finite number of identical and energetically equivalent active sites in which there is no lateral interaction between adsorbed species. Linearized Langmuir equation is as follows:

$$\frac{C_e}{q_e} = \frac{1}{Q_{\max} \times b} + \frac{C_e}{Q_{\max}} \qquad (4)$$

Where, q_e (mg g^{-1}) the equilibrium adsorption capacity, Q_{max} (mg g^{-1}) is the maximum monolayer

adsorption capacity, and b (mg L^{-1}) is the Langmuir adsorption constant representing site affinity.

The graph of C_e/q_e versus C_e was highly linear, and the correlation coefficient was high (R^2 = 0.9934), which demonstrates that the Langmuir model is best fitted and suitable to explain the Cd^{+2} adsorption onto Sr-Cu@g-C_3N_4, as depicted in Fig. 3b. This value of Q_{max} of about 178 mg g^{-1} is very close to the experimental value, and thus indicated the presence of a saturated monolayer of Cd^{+2} on the composite surface(Table 1). The high value of the b also highlights the high level of interaction between the Cd^{+2} and the active sites of the Sr-Cu@g-C_3N_4 composite. The Langmuir isotherm results strongly suggest that adsorption is predominantly physisorption driven with favorable binding.

3.3.3. Dubinine-Raduskevish Model (D-RM)

The Dubinin-Radushkevich isotherm is commonly used to differentiate between physical and chemisorption on the basis of the mean adsorption energy. Its linear form is given in eq 5:

$$\ln q_e = \ln X_m - \beta\varepsilon^2 \quad (5)$$

Here, q_e (mg g^{-1}) is the adsorption capacity, β (kJ^2 mol^{-2}) is related to adsorption mean energy, R is the general gas constant and ε^2 is the Polanyi potential value, which is calculated eq 6:

$$\varepsilon^2 = RT \ln\left(1 + \frac{1}{C_e}\right) \quad (6)$$

The mean energy of adsorption E (kJ mol^{-1}) was obtained by eq 7:

$$E = \frac{1}{\sqrt{2\beta}} \quad (7)$$

The D-R plot, as shown in Fig. 3c, has provided the correlation coefficient of R^2 =0.7950 and the estimated mean adsorption energy was about 127 kJ mol^{-1} which was within the chemisorption range (Table 1)(Zheng et al., 2024). This indicates that Cd^{+2} adsorption on Sr-Cu@g-C_3N_4 is mainly through ion-exchange or surface complexation instead of weak physisorption.

3.3.4. Elovich Model

The Elovich isotherm is commonly used to adsorption systems with heterogeneous surfaces where the number of sites available to adsorption grows exponentially [38]. Its linearized form is given in eq 8:

$$\ln\frac{q_e}{C_e} = \ln K_E Q_{max} - \frac{q_e}{Q_{max}} \quad (8)$$

In the above equation, Q_{max} is an adsorption capacity obtained from the Elovich linearization (mg g^{-1}) and K_E (L mg^{-1}) is the initial rate constant for the sorption process (Table 1).

The plot of $\ln(q_e/C_e)$ verses C_e, as shown in Fig. 3d, exhibited a fair degree of linearity with a correlation coefficient of R^2 = 0.9839 which showed that the Elovich model is partially applicable in explaining the Cd^{+2} adsorption behavior. Nevertheless, it does not fit as well as the Langmuir model, suggesting that, even in the presence of surface heterogeneity, monolayer adsorption is the prevalent process.

$$E = \frac{1}{\sqrt{-2\beta}} \quad (9)$$

Table.1 Different parameter obtained from isothermal modeling (linear form) for Cd^{+2} adsorption onto Sr-Cu@g-C_3N_4.

Isothermal Modeling	Parameters (Units)	Values
Freundlich	K_F= Q_{max}(mg g^{-1})	6.2446
	n	1.4146
	R^2	0.967
Langmuir	Q_{max}(mg g^{-1})	201.62
	b	-0.08338
	R^2	0.9957
Dubinine-Raduskevish	X_m= Q_{max}(mg g^{-1})	185.83
	β (kJ^2 mol^{-2})	$3.09x10^{-5}$
	E (kcal mol^{-1})	127.
	R^2	0.863
Elovich	Q_{max}(mg g^{-1})	507
	K_E (L mg^{-1})	0.00598
	R^2	0.9839

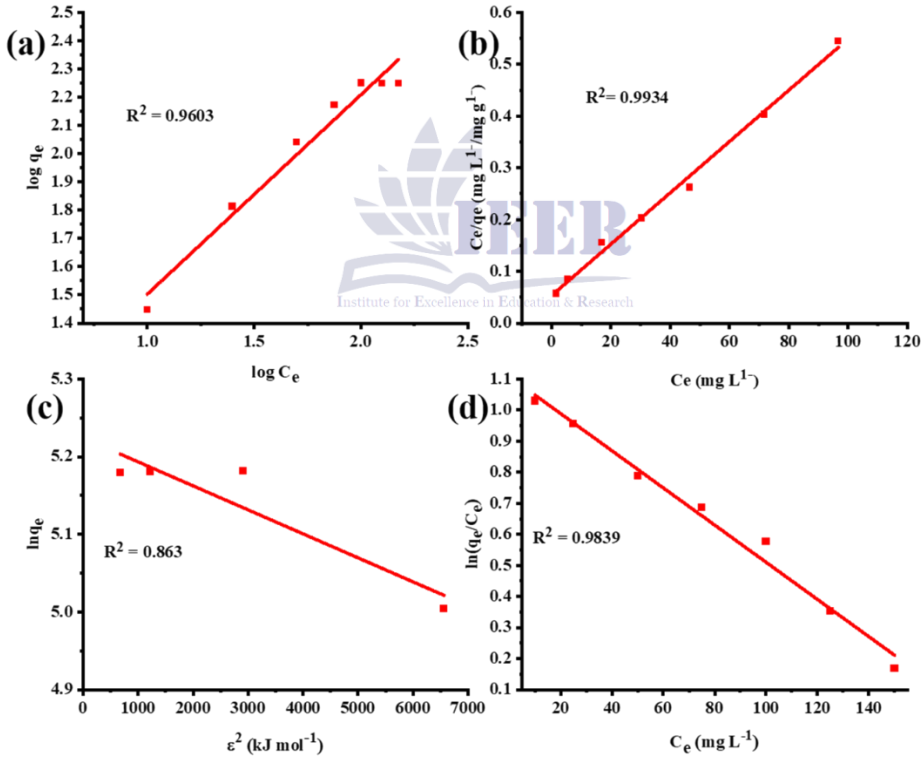

Figure 4. Fitting of Isothermal models (linear form) (a) Freundlich (b) Langmuir (c) Dubinine-Raduskevish model and (d) Elovich model on Cd^{+2} adsorption onto Sr-Cu@g-C_3N_4 composite.

3.4. Kinetic Modeling

To explain the adsorption kinetics and to determine the rate-limiting mechanism dominating the uptake process of Cd^{+2} onto the synthesized sorbent, the experimental kinetic data were subjected to analysis using various classical models: the pseudo-first-order, pseudo-second-order, intra-particle diffusion, and pore diffusion. Only the linearized forms of these models are explained.

3.4.1. Pseudo-First-Order Kinetic Model.

The pseudo-first-order kinetic model is often used to assess the adsorption processes in regard to whether the adsorption of the solute molecules onto the adsorbent surface is controlled by the bulk diffusion to the external surface of the adsorbent. The pseudo-first-order form of kinetic model is in a linear form and it is given in eq 9:

$$\log\left(q_e - q_t\right) = \log q_e - \frac{k_1}{2.303} t \qquad (9)$$

Where, q_e (mg g^{-1}) and q_t (mg g^{-1}) are the amount of Cd^{+2} adsorbed at point of equilibrium at time t (min), respectively, and k_1 (min^{-1}) is the rate constant of the pseudo-first-order reaction (Table 2).

Fig. 4a, indicates a linear relationship between the log, q_e- q_t verses t, but the correlation coefficient (R^2=0.9575) is relatively small compared to other kinetic models. Besides, the equilibrium adsorption capacity (q_e) obtained through intercept is very different with the corresponding experiment value (178 mg g^{-1}). This difference shows that a pseudo-first-order model cannot be used to characterize the Cd^{+2} adsorption kinetics in this system. The pseudo-first-order kinetic model suggests that surface diffusion serves as the rate-limiting step for adsorption.

3.4.2. Pseudo Second Order Kinetic Model

The pseudo second order kinetic model is the most common model employed in attempts to describe the adsorption processes that are dominated by chemisorption processes which involve the adsorption of the substance through the valence forces involving the sharing of electrons or the exchange of electrons between the adsorbate and the adsorbent. The linearized pseudo-second order kinetic is represented in eq 10:

$$\frac{t}{q_t} = \frac{1}{k_2 q_e^2} + \frac{t}{q_e} \qquad (10)$$

Where, k_2 (g mg^{-1} min^{-1}) is the pseudo-second order rate constant.

As shown in Fig. 4b, plot is highly linear with a high regression coefficient (R^2 = 0.9957). The slope determined the equilibrium adsorption capacity is close to the experimental sorption capacity (178 mg g^{-1}), which shows that this model fit the best (Table 2). The better fit of the pseudo-second-order model indicates that the adsorption of the Cd^{+2} onto the Sr-Cu@g-C_3N_4 is mainly determined by chemisorption through valence forces or the exchange of electrons between the Sr-Cu@g-C_3N_4 surface and the Cd^{+2} (Abia & Asuquo, 2008).

3.4.3. Intra-Particle Diffusion.

Intra-particle diffusion model is commonly used to assess the adsorption process to determine whether or not the entire process is governed by surface adsorption or whether diffusion of adsorbate species in the inner-pores of the Sr-Cu@g-C_3N_4 also had a considerable influence. The Weber-Morris model states that when a graph of the amount adsorbed at time t (q_t) versus the square root of time ($t^{1/2}$) generates a straight line with the origin, then intra-particle diffusion is the only rate-limiting process. However deviation from the origin indicates that there may be more than one adsorption process at the same time.

The linearized form of intra-particle diffusion model is given in eq 11:

$$q_t = k_{idm} t^{1/2} + C \qquad (11)$$

Where, k_{idm} (mg g^{-1} $min^{-1/2}$) is the intraparticle diffusion rate constant, C (mg g^{-1}) the thickness of the boundary layer, also referred to as the Weber-Morris constant.

The intra-particle diffusion plot of Cd^{+2} adsorption is given in Fig. 4c, which showed that the entire process occurred in two stages in linear fashion, meaning that there were more than one rate-limiting step in the entire process of adsorption.

Stage 1 showed a sharp linear region with comparatively high rate constant diffusion, meaning that the uptake of Cd^{+2} was fast. This step is explained by the direct contact of Cd^{+2} with sufficiently active sites on the external surface of Sr-Cu@g-C_3N_4. The large value of k_{idm1} indicates a high-driving force at the start since the concentration gradient between the aqueous phase and sorbent surface is high, leading to rapid surface adsorption (Table 2). During stage 2 the slope of the plot was significantly lower, and k_{idm2} was also much lower. This phase is the slow adsorption of Cd^{+2} into the internal pore of Sr-Cu@g-C_3N_4. The larger value of the intercept (C_2) in this area indicates that the effect

of the diffusion layers is more significant in this area. It was assumed that the R_2^2 was increased in this stage, which leads to the assumption that it is a better linear model, and thus, pore diffusion becomes important in later adsorption stages.

No point in either of the linear regions went through the origin, so intra-particle diffusion cannot be discussed as the only rate-limiting step of Cd^{+2} adsorption. Rather the total process of adsorption is dominated by a sum of the surface adsorption followed by slow intra-particle diffusion.

3.4.4. Pore Diffusion Model

The pore diffusion model studies the diffusion of sorbate into the internal cavities of the adsorbent material, which may serve as a rate-controlling step for the kinetics of adsorption. Pore diffusion of Cd^{+2} adsorption was estimated by the linearized Bangham model, which is given in eq 12.

$$q_t = \ln k_B + \alpha_B \ln t \quad (12)$$

In this equation, q_t (mg g^{-1}) is the amount of Cd^{+2} that adsorbs with time (t), k_B (mg g^{-1}) is the Bangham constant of adsorption capacity, α_B (min^{-1}) is the pore diffusion constant (Table).

A linear plot of lnq_t versus lnt, as presented in Fig. 4d, was found to be linear, with a correlation coefficient R^2=0.9748. The value of α_B obtained was less than unity and this indicated that pore diffusion contributes significantly to the Cd^{+2} adsorption process. But the fact that the plot has been deviated is an indication that pore diffusion is not the only limiting step. Rather, adsorption is a multi-step reaction, with surface adsorption being the most important at early phases, and diffusion of adsorbate in the pores taking place later. This action reflects good use of the internal pore structure of the Sr-Cu@g-C_3N_4 in Cd^{+2} removal.

Table.2 Different parameters obtained from kinetic modeling (linear form) for Cd^{+2} sorption onto Sr-Cu@g-C_3N_4.

Kinetics Modeling	Parameters (Units)	Values
Pseudo-first-order	k_1 (min^{-1})	0.158934
	R^2	0.9325
Pseudo-second-order	Q_{max}(mg g^{-1})	194.4
	k_2 (g $mg^{-1}min^{-1}$)	0.001494
	R^2	0.996339
Intra-vertical diffusion	k_{idm1} (mg g^{-1} $min^{-1/2}$)	31
	R_1^2	0.9788
	C_1 (mg g^{-1})	28
	k_{idm2} (mg g^{-1} $min^{-1/2}$)	1.72
	R_2^2	0.983
	C_2 (mg g^{-1})	165
Pore diffusion	α_B (min^{-1})	0.34590706
	R^2	0.9748

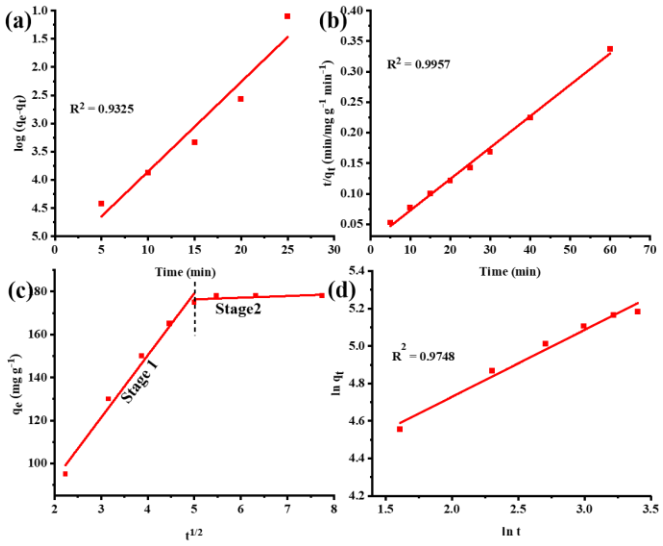

Figure.5. Fitting of Kinetic Models (Linear form) (a) pseudo-first-order (b) pseudo-second-order (c) intra-particle diffusion and (d) pore diffusion model for Cd^{+2} adsorption onto the synthesized Sr-Cu@g-C_3N_4 composite.

3.5. Thermodynamic study

The thermodynamic parameters of the Cd^{+2} adsorption onto the synthesized Sr-Cu@g-C_3N_4 sorbent were measured in order to explain the feasibility of the sorption process, the nature of the mechanistic process, and the temperature dependency of the sorption process. Equilibrium data at various temperatures were obtained to draw ΔG^0, ΔH^0 and ΔS^0. The distribution coefficient (K_c) was calculated as the ratio of amount of Cd^{+2} adsorbed to the amount left in solution and the ΔG^0 of the reaction was then calculated by following eq 13:

$$\Delta G^o = -RT \ln K_c \quad (13)$$

Where, R represents the general gas constant (8.314 J mol^{-1} K^{-1}), T is expressed as the absolute temperature in Kelvin, and K_c is the distribution coefficient, obtained by the by the following eq 14:

$$K_c = \frac{q_e}{C_e} \quad (14)$$

Where, C_{ads} is the surface concentration of the sorbate on the Sr-Cu@g-C_3N_4 and C_e is the equilibrium concentration of the sorbate in the continuous aqueous phase. The ΔH^0 and ΔS^0 were then determined by the Van't Hoff relationship into the standard linear form (15):

$$\ln K_c = \frac{\Delta S^o}{R} - \frac{\Delta H^o}{RT} \quad (15)$$

The negative ΔG^0 values at all temperatures investigated proved the spontaneous nature of Cd^{+2} adsorption onto the Sr-Cu@g-C_3N_4. The magnitude of ΔG^0 was also found to be less in higher temperatures which means that lower temperatures preferred the adsorption process. The negative value of $\Delta H°$ indicated an exothermic adsorption, which was in line with the decrease in the adsorption capacity with high temperatures, as shown in Fig. 6a. In addition, the $-\Delta S^0$ indicates that there was a reduction in the randomness at the solid solution interface when Cd^{+2} was adsorbed, which denoted the ordered arrangement of the Cd^{+2} on the Sr-Cu@g-C_3N_4 surface (Table 3).

On the whole, thermodynamic data supports the batch adsorption experiments and proves that the Cd^{+2} removal by the synthesized Sr-Cu@g-C_3N_4 sorbent is a spontaneous, exothermic, and thermodynamically viable process, with a higher affinity at lower temperatures.

Table. 3. Thermodynamic parameters for Cd^{+2} adsorption onto the synthesized Sr-Cu@g-C_3N_4 composite.

Model	Parameters	Values
Thermodynamics	R^2	0.9989
	$\Delta H°$ (kJ mol^{-1})	−18.4
	$\Delta G°$ (kJ mol^{-1})	− 7.12
	$\Delta S°$ (J mol^{-1} K^{-1})	- 38.2

3.6. Adsorption Mechanism

The Cd^{+2} adsorption process on the sorbent follows a synergistic interaction between physical and chemical interactions. First, the Cd^{+2} are transferred from aqueous solution to the sorbent surface by the electrostatic interaction and concentration mass transfer. This is followed by intense interactions between Cd^{+2} and surface functional groups such as hydroxyl (OH^-), carboxylic (COOH) and amine (NH_2) groups by ion exchange and surface complexation. During the adsorption process, the diffusion of Cd^{+2} into the inner pores of the Sr-Cu@g-C_3N_4 occurs, and it is controlled by intraparticle and pore diffusion. The nature of pseudo-second-order kinetics implies that chemisorption is the regulating process. In general, the adsorption process follows a surface complexation process and a diffusion-controlled transport process until an equilibrium is achieved.

3.7. Regeneration Study

The reusability of the sorbent was tested in five consecutive adsorption-desorption cycles, the respective sorption efficiencies are represented in Fig. 6b. The sorbent exhibited high initial Cd^{+2} removal efficiency of about 92% in the first cycle, which is an indication of a high affinity to Cd^{+2}. Following cycles showed that there was a progressive decline in sorption efficiency, whereby, it reduced to about 89, 86, 82, and 78% in the second, third, fourth, and fifth cycle respectively.It is possible that the measured decrease in the adsorption efficiency of the consecutive regeneration cycles could be explained by the incomplete desorption of the Cd^{+2}, partial blockage or loss of the active sites, and slight structural changes of the sorbent during repeated use. However, the sorbent also showed high structural stability and regeneration capacity after five cycles to retain over 75% of its original adsorption capacity. These findings verify the economic and practical viability of the synthesized sorbent to be reused in the removal of Cd^{+2} in wastewater systems.

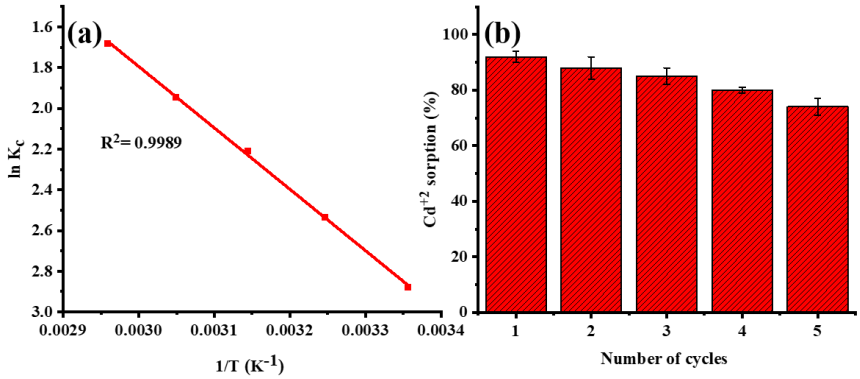

Figure. 6. (a) Effect of temperature for Cd^{+2} adsorption onto the synthesized Sr-Cu@g-C_3N_4 composite. (b) Regeneration result showing the efficiency of Sr-Cu@g-C_3N_4 composite for Cd^{+2} adsorption.

4. Conclusion

Under optimum conditions, the Sr-Cu@g-C_3N_4 composite was very efficient in removing Cd^{+2} in aqueous media. Optimum conditions were achieved by using a sorbent dose of 30 mg, initial concentration of 100mg of Cd^{+2} and a contact time of 30 min at a temperature of 298K. The material exhibited a highest sorption capacity of about 178 mg g^{-1}, which showed high metal-sorbent interactions. The Langmuir isotherm was best used to describe adsorption equilibrium, which showed that a monolayer of Cd^{+2} was covered. Kinetic experiments showed a high level of consistency with the pseudo-second-order model, which implies chemisorption-controlled uptake. Diffusion experiments showed that it is a multi-step process with surface adsorption, intraparticle diffusion, and pore diffusion. The nature of the process was proven to be spontaneous and exothermic by thermodynamic parameters. The sorbent had a high adsorption efficiency even after several regeneration cycles, which shows its stability. These results show that Sr-Cu@g-C_3N_4 has the potential to be a reused and promising adsorbent in Cd^{+2} contaminated wastewater.

REFERENCE

[1] Zhang, Y., Shen, Z., Zhou, W., Liu, C., Li, Y., Ding, B., Zhang, P., Zhang, X. and Zhang, Z., 2024. Environmental problems of emerging toxic metals and treatment technology and methods. *RSC advances*, *14*(50), 37299-37310.

[2] Houessionon, M.K., Ouendo, E.M.D., Bouland, C., Takyi, S.A., Kedote, N.M., Fayomi, B., Fobil, J.N. and Basu, N., 2021. Environmental heavy metal contamination from Electronic Waste (e-waste) recycling activities worldwide: A systematic review from 2005 to 2017. *International Journal of Environmental Research and Public Health*, *18*(7), 3517.

[3] Ma, Y., Su, Q., Yue, C., Zou, H., Zhu, J., Zhao, H., Song, R. and Liu, Z., 2022. The effect of oxidative stress-induced autophagy by cadmium exposure in kidney, liver, and bone damage, and neurotoxicity. *International Journal of Molecular Sciences*, *23*(21), 13491.

[4] Singh, T., & Majumder, C. (2015). Singh, T. and Majumder, C.B., 2015. Kinetics for removal of fluoride from aqueous solution through adsorption from mousambi peel, ground nut shell and neem leaves. *Inter J Sol SciEngin Technol*, *3*(4), 879-883.

[5] Ali, A., Akram, A., Bakar, M.A., Amin, H.M., Zohra, L., Abbas, A., Sher, M., Hussain, M.A., Haseeb, M.T. and Imran, M., 2025. A model batch and column study for Cd (II) uptake using citric acid cross-linked *Salvia spinosa* hydrogel: Optimization through Box-Behnken design. Journal of Industrial and Engineering Chemistry, 151, 746-761.

[6] Hussain, A., Fatima, S., Abbas, A., Ali, A., Amin, M., Muhammad, G. and Sher, M., 2023. Removal of Cr (III) and Ni (II) from aqueous solution using a mixed cellulose ether-ester hydroxyethylcellulose adipate. Desalination and Water Treatment, 283, 153-163.

[7] Hussain, M.A., Gul, S., Abbas, A., Ali, A. and Alotaibi, N.F., 2021. Chemically modified rhamnogalacturonans from linseed: a supersorbent for Cd^{2+} and Pb^{2+} uptake from aqueous solution. Desalination and Water Treatment, 221, 163-175.

[8] Shehzad, M.K., Ali, A., Qasim, S., Mumtaz, A., Hussain, M.A., Fawy, K.F., Nishan, U., Azhar, I., Abbas, M.A. and Abba, A., 2025. Sustainable remediation of cadmium using succinate-functionalized glucoxylan from chia (*Salvia hispanica*) seeds hydrogel. Journal of Industrial and Engineering Chemistry. https://doi.org/10.1016/j.jiec.2025.10.034

[9] Ali, A., Haseeb, M.T., Hussain, M.A., Tulain, U.R., Muhammad, G., Azhar, I., Hussain, S.Z., Hussain, I. and Ahmad, N., 2023. A pH responsive and superporous biocomposite hydrogel of *Salvia spinosa* polysaccharide-co-methacrylic acid for intelligent drug delivery. RSC Advances, 13(8), 4932-4948.

[10] Ali, A., Hussain, M.A., Haseeb, M.T., Farid-Ul-Haq, M., Erum, A. and Hussain, M., 2024. Acute toxicity studies of methacrylic acid based composite hydrogel of *Salvia spinosa* seed mucilage: a potential non-toxic candidate for drug delivery. Cellulose Chemistry and Technology, 58(1-2), 45-53.

[11] Ali, A., Hussain, M.A., Haseeb, M.T., Tulain, U.R., Farid-ul-Haq, M., Tabassum, T., Muhammad, G., Hussain, S.Z., Hussain, I. and Erum, A., 2023. Synthesis, characterization, and acute toxicity of pH-responsive *Salvia spinosa* mucilage-co-acrylic acid hydrogel: A smart excipient for drug release applications. Reactive and Functional Polymers, 182, 105466.

[12] Ali, A., Hussain, M.A., Abbas, A., Khan, T.A., Muhammad, G., Haseeb, M.T. and Azhar, I., 2022. Comparative isoconversional thermal analysis and degradation kinetics of *Salvia spinosa* (Kanocha) seed hydrogel and its acetates: a potential matrix for sustained drug release. Cellulose Chemistry Technolog, 56(3-4), 239-250.

[13] Ali, A., Hussain, M.A., Haseeb, M.T., Ashraf, M.U., Farid-ul-Haq, M., Tabassum, T., Muhammad, G. and Abbas, A., 2023. pH-responsive, hemocompatible, and non-toxic polysaccharide-based hydrogel from seeds of *Salvia spinosa* L. for sustained release of febuxostat. Journal of the Brazilian Chemical Society, 34, 906-917.

[14] Rehman, A.U., Maqsood, A., Siddique, A.B., Akhtar, S., Fawy, K.F., Ain, Q.U., Sher, M., Nishan, U., Ahmad, T., Ali, A. and Abbas, A., 2025. From waste to water treatment: Banana peel powder for polystyrene removal with FTIR-based mechanistic understanding. Journal of Industrial and Engineering Chemistry. https://doi.org/10.1016/j.jiec.2025.11.036

[15] Ali, A., Hussain, M.A., Haseeb, M.T., Bukhari, S.N.A., Tabassum, T., Farid-ul-Haq, M. and Sheikh, F.A., 2022a. A pH-responsive, biocompatible, and non-toxic citric acid cross-linked polysaccharide-based hydrogel from *Salvia spinosa* L. offering zero-order drug release. Journal of Drug Delivery Science and Technology, 69, 103144.

[16] Amjad, F., Ali, A., Hussain, M.A., Haseeb, M.T., Ajaz, I., Farid-ul-Haq, M., Hussain, S. Z. and Hussain, I., 2025. A superabsorbent and pH-responsive copolymer-hydrogel based on glucomannans from *Ocimum basilicum* (sweet basil): A smart and non-toxic material for intelligent drug delivery. International Journal of Biological Macromolecules, 315(2), 144452.

[17] Ali, A., Haseeb, M.T., Hussain, M.A., Muhammad, T., Muhammad, G., Ahmad, N., Alotaibi, N.F., Hussain, S.Z. and Hussain, I., 2022. Extraction optimization of a superporous polysaccharide-based mucilage from *Salvia spinosa* L. Cellulose Chemistry and Technology, 56, 957-969.

[18] Iqbal, J., Kanwal, M., Siddique, A., Fawy, K.F., Sher, M., Nishan, U., ur Rehman, M.F., Abbas, M.A., Ali, A. and Abbas, A., 2025. β-Cyclodextrin-functionalized silver nanoparticles as a visual probe for selective tetrahydrocannabinol detection via host–guest induced plasmonic shifts. Microchemical Journal, 116177.

[19] Hussain, M.A., Shahzad, K., Ali, A., Haseeb, M.T. and Hussain, S.Z., 2025. Development of a novel smart bio-composite hydrogel based on dextran, citric acid, and glucoxylan for pH-dependent drug delivery and stimuli-responsive swelling and release. Polymers and Polymer Composites, 33, .09673911251350240.

[20] Zheng, C., Xie, Y., Niu, Y., Wang, C., Hu, J., Kang, K., Song, H. and Bai, S., 2024. Modeling of multi-temperature Type I and II benzene/ammonia adsorption isotherms: Dual LF model and linearized DR model. *Separation and Purification Technology*, *338*, 126246.

[21] Li, A., Lin, R., Lin, C., He, B., Zheng, T., Lu, L. and Cao, Y., 2016. An environment-friendly and multi-functional absorbent from chitosan for organic pollutants and heavy metal ion. *Carbohydrate polymers*, *148*, 272-280.

[22] Qian, X., Li, W., Wang, X., Guan, H., Bao, Q., Zhao, B., Wulan, B., Liu, S., Zhu, D., Feng, X. and Sun, J., 2025. Multifunctional roles of ionic microenvironments in the preparation, modification, and application of g-C3N4. *Advanced Functional Materials*, *35*(11), 2416946.

[23] Rajoria, S., Vashishtha, M. and Sangal, V.K., 2022. Treatment of electroplating industry wastewater: a review on the various techniques. *Environmental Science and Pollution Research*, *29*(48), 72196-72246.

[24] Raza, A., Haidry, A.A., Yao, Z., Saleem, M.F., Alothman, A.A. and Mohammad, S., 2024. Synergistic effect of CuO and Sr doped g-C3N4 for CO2 photoreduction into hydrocarbon fuels. *Chemical Engineering Journal*, *480*, 148162.

[25] Revellame, E.D., Fortela, D.L., Sharp, W., Hernandez, R. and Zappi, M.E., 2020. Adsorption kinetic modeling using pseudo-first order and pseudo-second order rate laws: A review. *Cleaner Engineering and Technology*, *1*, 100032.

[26] Khatoon, M., Ali, A., Hussain, M.A., Haseeb, M.T., Muhammad, G., Sher, M., Hussain, S.Z., Hussain, I. and Iqbal, M., 2025. A chia (*Salvia hispanica* L.) seed mucilage-based glucoxylan-grafted-acrylic acid hydrogel: a smart material for pH-responsive drug delivery systems. Materials Advances, 6(8), 2636-2647.

[27] Hussain, M.A., Raees, N., Ali, A., Tayyab, M., Muhammd, G., Uroos, M. and Batool, M., 2025. Optimization of rhamnogalacturonan extraction from linseed using RSM and designing a pH-responsive tablet formulation for sustained release of ciprofloxacin. Cellulose Chemistry and Technology, 59, 547-558.

[28] Hussain, M.A., Taj, T., Ali, A., Haseeb, M.T., Hussain, S.Z., Muhammad, G. and Bukhari, S.N.A., 2025. Cross-Linking of Hydroxypropylcellulose With Flaxseed Rhamnogalacturonans Using Citric Acid Produces a Hemocompatible Biocomposite for pH-Responsive Rifaximin Delivery. Journal of Applied Polymer Science, e57486.

[29] Hussain, M.A., Abbas, A., Yameen, E., Ali, A., Muhammad, G., Hussain, M. and Shafiq, Z., 2022. Adsorptive removal of Pb^{2+} and Cu^{2+} from aqueous solution using an acid modified glucuronoxylan-based adsorbent. Desalination and Water Treatment, 248, 163-175.

[30] Hussain, M.A., Abbas, A., Habib, M.G., Ali, A., Farid-ul-Haq, M., Hussain, M., Shafiq, Z. and Irfan, M.I., 2021. Adsorptive removal of Ni (II) and Co (II) from aqueous solution using succinate-bonded polysaccharide isolated from Artemisia vulgaris seed mucilage. Desalination and Water Treatment, 231, 182-195.

[31] Ali, A., Hussain, M.A., Abbas, A., Haseeb, M.T., Azhar, I., Muhammad, G., Hussain, S.Z., Hussain, I. and Alotaibi, N.F., 2023. Succinylated *Salvia spinosa* hydrogel: Modification, characterization, cadmium-uptake from spiked high-hardness groundwater and statistical analysis of sorption data. Journal of Molecular Liquids, 376, 121438.

[32] Molaei, P. and Rahimi-Moghadam, F., 2021. Porous g-C3N4 nanosheets through facile thermal polymerization of melamine in the air for photocatalyst application. *Journal of Materials Science: Materials in Electronics*, *32*(14), pp.19655-19666.

[33] Khan, F., Siddique, A.B., Irfan, M.I., Hassan, M.N.U., Sher, M., Alhazmi, H.A., Qramish, A.N., Amin, H.M., Qadir, R. and Abbas, A., 2024. Maleated hydroxyethyl cellulose for the efficient removal of Cd (II) ions from an aqueous solution: isothermal, kinetic and regeneration studies. *Water, Air, & Soil Pollution*, *235*(8), 536.

[34] Nigar, H., Navascués, N., De La Iglesia, O., Mallada, R. and Santamaría, J., 2015. Removal of VOCs at trace concentration levels from humid air by Microwave Swing Adsorption, kinetics and proper sorbent selection. *Separation and Purification Technology*, *151*, 193-200.

[35] Li, W., Gu, G., Bi, C., Yang, S., Wang, Y., Peng, C. and Li, Y., 2025. The dual selective adsorption mechanism on low-concentration Cu (II): Structural confinement and bridging effect. *Journal of Hazardous Materials*, *489*, 137506.

[36] Zhang, B.L., Qiu, W., Wang, P.P., Liu, Y.L., Zou, J., Wang, L. and Ma, J., 2020. Mechanism study about the adsorption of Pb (II) and Cd (II) with iron-trimesic metal-organic frameworks. *Chemical Engineering Journal*, *385*, 123507.

[37] Ghosal, P.S. and Gupta, A.K., 2017. Development of a generalized adsorption isotherm model at solid-liquid interface: A novel approach. *Journal of Molecular Liquids*, *240*, 21-24.

[38] Liu, W., Wang, T., Borthwick, A.G., Wang, Y., Yin, X., Li, X. and Ni, J., 2013. Adsorption of Pb2+, Cd2+, Cu2+ and Cr3+ onto titanate nanotubes: Competition and effect of inorganic ions. *Science of the Total Environment*, *456*, 171-180.